Atmos. Chem. Phys. Discuss., 9, 26833–26880, 2009
www.atmos-chem-phys-discuss.net/9/26833/2009/

Atmospheric Chemistry and Physics Discussions

This discussion paper is/has been under review for the journal Atmospheric Chemistry and Physics (ACP). Please refer to the corresponding final paper in ACP if available.

Process analysis and sensitivity study of regional ozone formation over the Pearl River Delta, China, during the PRIDE-PRD2004 campaign using the CMAQ model

X. Wang[1], Y. Zhang[1], Y. Hu[2], W. Zhou[1,*], K. Lu[1], L. Zhong[3], L. Zeng[1], M. Shao[1], M. Hu[1], and A. G. Russell[2]

[1]State Joint Key Laboratory of Environmental Simulation and Pollution Control, College of Environmental Sciences and Engineering, Peking University, Beijing, China
[2]School of Civil and Environmental Engineering, Georgia Institute of Technology, Atlanta, Georgia, USA
[3]Guangdong Provincial Environmental Monitoring Center, Guangzhou, China

*now at: Department of Civil and Environmental Engineering, Rice University, Houston, Texas, USA

Received: 22 October 2009 – Accepted: 3 December 2009 – Published: 15 December 2009

Correspondence to: Y. Zhang (yhzhang@pku.edu.cn)

Published by Copernicus Publications on behalf of the European Geosciences Union.

Abstract

In this study, the Community Multiscale Air Quality (CMAQ) modeling system is used to simulate the ozone (O_3) episodes during the Program of Regional Integrated Experiments of Air Quality over the Pearl River Delta, China, in October 2004 (PRIDE-PRD2004). The simulation suggests that O_3 pollution is a regional phenomenon in the PRD. Elevated O_3 levels often occurred in the southwestern inland PRD, Pearl River estuary (PRE), and southern coastal areas during the 1-month field campaign. Three evolution patterns of simulated surface O_3 are summarized based on different near-ground flow conditions. More than 75% of days featured interaction between weak synoptic forcing and local sea-land circulations. Integrated process rate (IPR) analysis shows that photochemical production is the dominant contributor to O_3 enhancement from 09:00 to 15:00 LST (local standard time) in the atmospheric boundary layer over most areas with elevated O_3 occurrence in the mid-afternoon. The simulated ozone production efficiency is 2–8 O_3 molecules per NO_x molecule oxidized in areas with high O_3 chemical production. Precursors of O_3 originating from different source regions in the central PRD are mixed during transport to downwind rural areas during nighttime and early morning, where they then contribute to the daytime O_3 photochemical production. Such close interactions among precursor emissions, transports, and O_3 photochemical production result in the regional O_3 pollution over the PRD. Sensitivity studies suggest that O_3 formation is volatile organic compound-limited in the central inland PRD, PRE, and surrounding coastal areas with less chemical aging ($NO_x/NO_y>0.6$), but is NO_x-limited in the rural southwestern PRD with photochemically aged air ($NO_x/NO_y<0.3$).

1 Introduction

Tropospheric ozone (O_3) is a secondary pollutant produced through a series of photochemical reactions involving mainly nitrogen oxides (NO_x) and volatile organic

ACPD

9, 26833–26880, 2009

compounds (VOCs) in the presence of sunlight. Elevated concentration of ground-level O_3 is of great environmental concern due to its adverse impacts on human health and ecosystems, as well as its greenhouse effect (NARSTO, 2000).

The Pearl River Delta (PRD) is one of the most urbanized and industrialized regions in southern China. This area contains three megacities (Guangzhou, Shenzhen, and Hong Kong) and numerous medium and small cities, houses 4% of the total population of China, and produces about 19% of China's gross domestic product. As a consequence of the substantial economic development and increases in air pollutant emissions, in recent years, the PRD has experienced rapid deterioration of air quality. Photochemical smog has been one of the most severe air quality issues in the PRD, where surface O_3 levels exceeding the national hourly standard of 200 $\mu g/m^3$ (~0.093 ppm) are frequently observed by air quality monitoring networks, especially in fall when northerly winds and clear sky conditions prevail (Wang et al., 2001, 2003; Zhang et al., 2007, 2008a).

The O_3 pollution in Hong Kong has drawn much attention over the past decade. Meteorological conditions have been found to be closely associated with O_3 pollution in Hong Kong and the Pearl River estuary (PRE) area. The synoptic systems related to O_3 episodes in Hong Kong have been classified into three patterns: tropical cyclones, continental anticyclones, and low-pressure troughs (Huang et al., 2005, 2006; Chan and Chan, 2000). The impacts of the complex topography, local circulations, and low mixing height on heavy O_3 pollution were investigated (Liu and Chan, 2002; Ding et al., 2004; Lam et al., 2005), and a conceptual model was developed to explain the effect of land-sea breezes on pollutant transport, trapping, and accumulation (Lo et al., 2006). In addition, the local versus regional contributions to O_3 episodes in Hong Kong have been widely discussed using chemical transport models (CTMs) and a backward trajectory method (Ding et al., 2004; Lam et al., 2005; Huang et al., 2005, 2006; Wang et al., 2006; Zhang et al., 2007). The relative importance of local production and of regional transport from inland parts of the PRD was found to change under the different meteorological conditions controlling O_3 episodes as well as at different locations. Previous

ACPD
9, 26833–26880, 2009

studies have also addressed the relationship between O_3 and its precursors. In Hong Kong, the photochemical formation of O_3 is generally believed to be VOC-limited (Chan and Yao, 2008).

However, O_3 pollution in the PRD region outside of Hong Kong and PRE has not yet been investigated adequately, and only limited studies have been reported. Wang et al. (2005) evaluated the importance of different emission sources on the concentrations of O_3 and other pollutants for the whole PRD in March 2001. Wei et al. (2007) investigated the impact of biogenic VOC emissions on O_3 formation. Zhang et al. (2008b) and Shao et al. (2009) adopted an observation-based model (OBM) to investigate O_3 production sensitivity to precursors in Guangzhou. The CTM is a fundamental tool for exploring the spatiotemporal evolution of O_3 pollution and assessing the roles of different atmospheric processes in O_3 formation. However, three-dimensional (3-D) modeling studies have rarely been performed to address these issues for O_3 episodes over the inland PRD region. Moreover, to develop effective strategies for O_3 pollution control, our understanding of O_3-VOC-NO_x chemistry over the whole PRD needs to be improved through more observational and modeling studies.

The Program of Regional Integrated Experiments of Air Quality over the Pearl River Delta, China, in October 2004 (PRIDE-PRD2004) produced a comprehensive database of O_3, particulate matter, and other air pollutant measurements in this region (Zhang et al., 2008a), providing an ideal testbed for application of a CTM to thoroughly investigate the spatiotemporal evolution and chemical characteristics of ground-level O_3 pollution over the whole PRD region.

In this paper, the US Environmental Protection Agency (EPA) Community Multiscale Air Quality (CMAQ) modeling system is applied to simulate O_3 episodes during the PRIDE-PRD2004 campaign. Our goal is to quantify the impacts of different chemical and physical processes on elevated O_3 formation and to characterize the regional O_3 chemical production over the entire PRD area. Section 2 describes the modeling methodology. Section 3 presents and discusses the model performance, the spatiotemporal evolution of elevated O_3, the influence of different processes on O_3

formation, and the characteristics of O_3 chemical production. A summary of conclusions is provided in Sect. 4.

2 Methodology

2.1 Model setup and inputs

We use CMAQ (version 4.5, Byun and Schere, 2006) with the Statewide Air Pollution Research Center version 99 (SAPRC-99) chemical mechanism (Carter, 2000) to simulate O_3 formation during the whole month of October 2004. The model is configured to have triple-nested domains (Fig. 1). The outer domain with a horizontal grid spacing of 36 km covers the entire area of China, the 12-km grid-spacing inner domain covers Guangdong, Hong Kong, and Macao, and the innermost domain with a 4-km horizontal grid resolution focuses on the PRD. All the grids have 13 layers vertically extending from the surface to an altitude of ~17 km above the ground, with seven layers below 1 km and the first layer height at ~19 m. The results from the 36-km outer domain are used to provide boundary conditions for the inner domains. A spin-up period of 3 days (1–3 October) is used in the CMAQ simulation to minimize the influence of initial conditions.

The fifth-generation Pennsylvania State University/National Center for Atmospheric Research (PSU/NCAR) Mesoscale Model (MM5, version 3.7) (Grell et al., 1994) is used to simulate the meteorological fields to drive CMAQ. MM5 is run with 34 vertical layers and with the following physics options: the mixed-phase microphysics, the Grell cumulus scheme, the medium-range forecast (MRF) model's boundary layer scheme, a rapid radiative transfer model (RRTM) longwave scheme, and the Noah land-surface model. The National Centers for Environmental Protection (NCEP) $1^\circ \times 1^\circ$ global reanalysis data, the NCEP global surface and upper air observation data, and observations in the atmospheric boundary layer (ABL) measured during the PRIDE-PRD2004 campaign are used to prepare the initial and boundary conditions for the MM5 simulations.

ACPD
9, 26833–26880, 2009

The four-dimensional data assimilation (FDDA) technique ("grid nudging") is used to nudge 3-D winds, temperature and humidity, and surface winds.

The gridded and speciated hourly emission inputs for CMAQ are prepared using the Sparse Matrix Operator Kernel Emissions (SMOKE) model (version 2.3, Houyoux et al., 2000). The TRACE-P anthropogenic emissions inventory (Streets et al., 2003) with a coarse resolution is used for the outer 36-km domain. Inventory inputs (to SMOKE) of anthropogenic emissions for the inner domains are based on an inventory compiled by the Hong Kong Environmental Protection Bureau (personal communication, 2006) as well as some results on local source emissions reported by recent studies in this area (Cao et al., 2005; Song and Xie, 2006; Liu et al., 2008a). In this composite and high-resolution regional inventory, anthropogenic emissions of NO_x, VOCs, CO, SO_2, NH_3, and PM are reported in three major source categories: point sources (mainly power generation and industrial sources), mobile sources (on-road and off-road vehicles, marine traffic, and aircraft), and area sources (e.g. domestic and commercial fuel combustion, industrial processes, solvent evaporation loss, storage and transport of petroleum products, and agricultural activities). The biogenic VOC and NO emissions are estimated by applying the Biogenic Emissions Inventory System version 3.09 (BEIS 3.09) with a Chinese plantation survey dataset.

As shown in Table 1, mobile sources and power generation point sources contribute about 47% and 40%, respectively, of the total NO_x emissions in the PRD, whereas mobile sources and evaporation losses of solvents and petroleum are the two largest contributors to VOC emissions, accounting for 49% and 31%, respectively. Spatially, both NO_x and VOC emissions are found to concentrate over the inland urban areas of Guangzhou, Foshan, and Dongguan; the coastal areas of Dongguan and Shenzhen; and the urban core of Hong Kong (Fig. 2).

2.2 Model evaluation protocol

Predicted meteorological fields (including winds, temperature, and humidity) over the PRD are examined against the hourly observations obtained during the field campaign.

ACPD
9, 26833–26880, 2009

Performance statistics for the MM5 simulations are calculated using the Metstat statistical analysis package (Emery et al., 2001).

The simulation of O_3 formation during 4–31 October is evaluated against observations made at two super sites of the PRIDE-PRD2004 campaign (Zhang et al., 2008a) and measurements collected simultaneously at the ten regular surface sites of the PRD air quality monitoring network (see site locations in Fig. 1b). Note that the platform of the super site at Guangdong Provincial Environmental Monitoring Center (GDEMC) sits on the roof of a 17-story building, ~50 m above the ground, in the urban center of Guangzhou City. The other super site of Xinken is a seaside rural site. Two kinds of measurement techniques for non-methane hydrocarbons (NMHCs) were applied at the super sites. One was canister sampling followed by analysis using gas chromatography (GC) combined with mass spectrometry (MS) and flame ionization detection (FID) for C2-C12 species (Liu et al., 2008b), and the other was on-line GC-FID for C3-C12 species (Wang et al., 2008a). The canister measurements usually collected three samples per day at GDEMC and two samples per day at Xinken during the entire campaign, whereas the on-line observations are only available in the second half of the month. The simulated concentrations of all NMHC-related species in the SAPRC99 mechanism are summed together for comparison with canister NMHCs observations, and C2 species are not included in the simulated values when those values are compared with the on-line NMHCs observations.

The performance is judged by statistical measures, including the correlation coefficient, normalized mean bias (NMB), and normalized mean error (NME), defined as

$$\mathrm{NMB}=\frac{\sum_{i=1}^{N}\left(C_i^s-C_i^o\right)}{\sum_{i=1}^{N}C_i^o}\times 100\%, \quad (1)$$

ACPD
9, 26833–26880, 2009

$$\mathrm{NME} = \frac{\sum_{i=1}^{N} \left| C_i^s - C_i^o \right|}{\sum_{i=1}^{N} C_i^o} \times 100\%, \quad (2)$$

where C_i^s and C_i^o represent simulated and observed concentrations at a same monitoring site for the same hour, respectively, and N is the total number of such data pairs of interest.

2.3 Integrated process rate analysis

Production of O_3 is the net result of interactions of the various atmospheric processes involved (e.g. chemistry, transport, deposition). The integrated process rate (IPR) analysis implemented in the CMAQ model is used here to investigate the influences of major physical processes and the net effect of chemistry on model predictions. The IPR analysis calculates hourly contributions of gas-phase chemistry (CHEM), horizontal transport (HTRA, including advection and diffusion), vertical transport (VTRA, including advection and diffusion), dry deposition (DDEP), and some other processes (such as cloud processes, aerosol processes, and emissions) at each model grid cell. Details of IPR analysis have been provided by Jeffries and Tonnesen (1994), Jang et al. (1995), and Gipson (1999). Recent applications of the IPR in CMAQ models have been reported by Xu et al. (2008), Yu et al. (2009), Goncalves et al. (2009), Wang et al. (2009), and Zhang et al. (2009a, b).

For the IPR analysis, we first assess the roles of various atmospheric processes in O_3 formation in the ABL at the two super sites, GDEMC and Xinken, as well as at Donghu station. The O_3 pollution at GDEMC represents a typical situation in Guangzhou urban areas (source region), whereas that at Xinken, a rural site with less local emissions, reflects the influences of pollutants transported from upwind areas (Guangzhou and Dongguan under northerly winds; Shenzhen and Hong Kong under

southerly winds). Donghu is an urban site in Jiangmen City, located ~60 km downwind of the urban areas of Guangzhou and Foshan under northerly wind conditions. The maximum O_3 levels were recorded at Donghu during the campaign. We then investigate the influences of different processes (precursor emissions, physical transport, and chemical process) on the formation and evolution of regional O_3 pollution over the PRD.

2.4 Ozone production efficiency calculation

Ozone production efficiency (OPE) is defined as the number of molecules of O_3 formed per NO_x removed from atmospheric ozone-forming oxidation cycles [i.e. $P(O_3)/P(NO_z)$] (Seinfeld and Pandis, 2006). OPE is an important measure for determining the efficiency of the catalyst NO_x in O_3 formation and for indicating the O_3-VOC-NO_x sensitivity under certain polluted conditions (Sillman, 1995; Sillman and He, 2002). In this work, OPE for the time range and spatial region of interest is estimated based on the IPR results, which provide the net chemical production of O_3 and NO_z at each grid cell on an hourly basis [i.e. $P(O_3)$ and $P(NO_z)$].

2.5 O_3 sensitivity testing

Understanding of the non-linear relationship between O_3 formation and its precursors is critical for the development of an effective O_3 control strategy. We evaluate the O_3 response to precursors by perturbing the domain-wide anthropogenic emissions of NO_x and VOCs and then examining the resulting changes in O_3 concentrations and O_3 production rates. The perturbations of emissions include a 25% reduction in NO_x emissions (N075V100), a 25% reduction in VOC emissions (N100V075), and a 25% reduction in both emissions (N075V075). The O_3 sensitivity to precursors may vary with the magnitude of emission reductions; here, 25% emission-reduction scenarios are used because this reduction level is more feasible and probable in real controls than 50% or higher reductions. Furthermore, we examine the influence of the photochemical

age of the air mass (indicated by the ratio of NO_x/NO_y) on the sensitivity of O_3 formation to precursors.

3 Results and discussions

3.1 Evaluation of model performance

Simulated surface meteorological fields are examined against surface hourly observations over the PRD during the field campaign, and the MM5 model performance (shown in Table 2) is well within the typical range for meteorological modeling (Emery et al., 2001; Hanna and Yang, 2001).

Simulated O_3 concentrations compare well against the observations at the two super sites and at other network sites (Table 3), with a correlation coefficient of 0.60, NMB of −17.4%, and NME of 26.4%, comparable to results of other CMAQ applications (Zhang et al., 2006; Goncalves et al., 2009). The simulations reproduce the diurnal variations and magnitude of O_3 reasonably well at most sites (Fig. 3), except at Tianhu, which is an upwind rural site. Comparisons of precursor concentrations (i.e. NO_2 and NMHCs) at monitoring sites further demonstrate that the O_3 formation is captured reasonably well (and for the right reasons) across over the domain and throughout the period (Figs. 4 and 5).

Note that levels of peak O_3 tend to be underpredicted at a few sites (e.g. Tianhu, Wanqingsha, and Zimaling, see Fig. 3). This may be related to several factors, such as the uncertainties in the precursor emissions and meteorological parameters. In the current inventory, compared with the data for PRD urban areas, the emission estimations over the suburban and rural areas of the PRD and the areas outside the PRD have higher uncertainties due to the limited source information available and fewer reported studies. For instance, the evolution of observed O_3 at Tianhu, a rural site in the far north of Guangzhou, had an elevated background level of O_3 ranging from 60 to 70 ppb during the campaign and was less affected by local photochemical production

(except during 29–31 October). Considering the prevailing northerly winds in October, the underestimations of O_3 at Tianhu may be caused by the uncertainties in emissions in northern rural areas of Guangzhou and distant northern areas such as Qingyuan. The overestimation of surface wind speeds by MM5 (see Table 2) may result in more transport and less accumulation of O_3 and its precursors, which is a probable cause of the underestimated O_3 peaks at some other sites as well.

3.2 Regional spatiotemporal evolution of surface ozone

Both the CMAQ simulation and air quality measurements demonstrate that the PRD experienced serious photochemical smog pollution at the regional scale during the campaign (Fig. 3). The simulated monthly average distribution indicates that elevated levels of surface O_3 usually occurred in the western and southern PRD. As shown in Fig. 6, areas with O_3 higher than 0.090 ppm include southern Foshan, Jiangmen, Zhongshan, the PRE and surrounding areas, and the southwestern coastal area. Regional O_3 pollution was also recorded at stations located in the western PRD and around the PRE, such as Donghu, Zimaling, Wanqingsha, Xinken, and Tung Chung, where the O_3 nonattainment (hourly O_3 concentration exceeding the national ozone air quality standard of 200 $\mu g/m^3$ or ~0.093 ppm) days accounted for 88%, 95%, 77%, 88%, and 61% of valid observation days during the campaign, respectively. The maximum hourly O_3 concentration of 0.179 ppm was measured at Donghu station (Zhang et al., 2008b). Although no surface observations of O_3 concentrations were conducted in central and western Jiangmen during the campaign, aircraft measurements in the ABL reported average O_3 levels of around 0.080 ppm and a maximum O_3 value of 0.101 ppm over Kaiping in the afternoon (close to the levels in Zhongshan, but higher than those in Foshan and Huizhou) (Wang et al., 2008b), suggesting the occurrence of O_3 pollution in the rural western PRD with low precursor emissions.

The formation and distribution of O_3 pollution over the PRD is greatly influenced by synoptic weather conditions and local circulations. During the campaign, a high-pressure system dominated over the PRD and resulted in light-to-moderate northerly

or northeasterly synoptic winds. Three cold air masses from the north intruded into the PRD on 1, 17, and 25 October. After the influence of cold air weakened, both meteorological observations and simulated results showed the evolution of sea-land breezes in the southern PRD. Under weak synoptic conditions, northeasterly/northerly/easterly winds were dominant over the PRD from early morning to midday, and southerly or southeasterly sea breezes usually began in afternoon and ended around midnight in the southern PRD (Fan et al., 2008).

Based on the influences of the different near-ground flow patterns, we summarize three evolution patterns of simulated surface O_3 over the PRD during the studied month. For the first category, the flow patterns in lower layers were characterized by northerly or northeasterly winds prevailing over the PRD during the whole day due to moderate or strong synoptic forcing resulting from the intrusion of northern cold air. Elevated O_3 during mid-afternoons were usually distributed over southwestern inland and coastal regions, as well as the PRE area. At dusk, O_3 concentrations in the urban areas of Guangzhou, Foshan, Shenzhen, and Hong Kong dropped to low levels due to the decrease in photochemical production and the removal of O_3 by NO titration and dry deposition, while continuous transport by northerly winds moved the O_3 plume to the southern water area (see Fig. 7a).

The other two patterns occurred when synoptic winds were weak and sea-land breezes showed important influence on the transport of air pollutants. Weak synoptic winds and stagnant conditions usually resulted in more severe photochemical pollution in the PRD. For the second category, northeasterly winds were dominant in the daytime over the PRD. Daytime elevated O_3 was mainly distributed in the southwestern inland regions, PRE, and southern coastal areas (Fig. 7b). Because a southeasterly sea breeze developed along the coastal areas and strengthened gradually during the afternoon and at dusk, transport of the O_3 plume to the southern water area was delayed, and O_3 remained at high levels in the southern rural land areas of Jiangmen and Guangzhou even after sunset. For the third pattern, the easterly winds prevailed in lower layers during the daytime over most areas, elevated O_3 usually occurred in

ACPD
9, 26833–26880, 2009

the western PRD in the afternoon, and high levels of O_3 were seldom found along the southern coastal area except for the PRE (Fig. 7c).

We group all days during 4–31 October into the aforementioned three patterns (Table 4). The classification of pollution days reflects the influence of the interaction between synoptic forcing and local circulations on the evolution of O_3 pollution over the PRD during the campaign.

3.3 Process analysis of O_3 formation

Here, 16–22 October is used for the IPR analysis because the PRD experienced all three O_3 pollution patterns during this period (see Table 4), and the CMAQ simulation shows good performance at most sites on these days. The observed maximum height of the daytime ABL was about 1200 m during the campaign (Fan et al., 2008), corresponding to the lowest seven layers in the CMAQ simulation. Therefore, our process analysis mainly focuses on the IPR results from layers 1 to 7.

3.3.1 Process analysis at the selected site locations

Figures 8 and 9 reveal the different roles of atmospheric processes in the evolution of O_3 at the grid cells of the GDEMC, Xinken, and Donghu sites. In the lower layers of the urban GDEMC site, the chemical process exhibited a significant consumption of O_3 during the whole day (especially during traffic rush hours) due to O_3 titration by high NO_x emissions, whereas horizontal and vertical transports were the main contributors to compensate for the chemical loss and to enhance the O_3 levels during the daytime (Fig. 8a). For the build-up of daytime maximum O_3 in the ABL from 09:00 to 15:00 LST (local standard time), the top chemical contributions occurred in the layers 5–7 (150–1000 m above ground level – a.g.l.); the produced O_3 was then horizontally transported to downwind areas and vertically transported to lower layers to balance the O_3 removal by NO titration and dry deposition (Fig. 9a).

At the rural Xinken site, O_3 was mainly contributed by vertical transport and then depleted on a similar magnitude by horizontal transport during the daytime (Fig. 8b). Such influences of transport processes may be associated with the circulations of sea-land breezes over the PRE. The analysis of the simulated 3-D air flows showed that local air circulations often occurred at Xinken and were characterized by downdraft in the upper layers and divergence in the lower layers (detailed discussion of this issue is presented in another manuscript prepared by Zhou et al., 2009: Land-sea breezes over Pearl River Estuary and their impact on local air quality in October 2004). The chemical process was also an important contributor to daytime O_3 enhancement, characterized by more O_3 production in lower layers (Fig. 9b).

Among the three sites (GDEMC, Xinken, and Donghu) shown in Fig. 9, Donghu experienced the maximum increase of O_3 concentration in the ABL from 09:00 (0.046 ppm) to 15:00 LST (0.121 ppm) (Fig. 9c). Chemical production dominated the O_3 enhancement, especially in upper layers (layers 3–7). In lower layers, although the influences of horizontal and vertical transports exhibited day-to-day variations due to different meteorological conditions, the net effects of transport mainly showed a positive contribution to near-ground O_3 in most hours of a day (Fig. 8c).

Dry deposition was another sink for surface O_3 at GDEMC and Donghu, but showed weaker effects at Xinken because water covers more than 90% of the grid cell in which this coastal site is located. The wet deposition and cloud processes were also negligible due to the low cloudiness and the absence of precipitation during this period.

In many O_3 chemistry studies, the total oxidant O_x (estimated by O_3+NO_2) is frequently used in data analysis because O_x is not affected by the rapid photodissociation of NO_2 and the titration of O_3 with NO, being a better measure of the real photochemical production of ozone (Chou et al., 2006; Zhang et al., 2008b). In layers 1–7, the overall average O_x chemical productions at GDEMC, Donghu, and Xinken were 0.102 ppm/6 h, 0.082 ppm/6 h, and 0.048 ppm/6 h, respectively, indicating that the photochemical oxidant production rate in the urban area was greater than that in the rural region, similar to findings from a study of O_3 pollution in Taipei (Chou et al., 2006). As shown in

ACPD
9, 26833–26880, 2009

Fig. 10, an interesting phenomenon is that the vertical profiles of O_x changes derived from gas-phase chemistry and accumulated from 09:00 to 15:00 LST were similar at GDEMC, Xinken, and Donghu (O_x chemical production decreases with height), in contrast to the significant differences among the vertical profiles of O_3 chemical formation illustrated in Fig. 9.

As pollutants are generally well mixed in the ABL during daytime conditions, we summarize the process budgets integrated over the depth of the daytime ABL (corresponding to the vertical range of layers 1 to 7) in Table 5. In the ABL, the process contributions to daytime maximum O_3 at GDEMC, Xinken, and Donghu share some common features regardless of their urban vs. rural locations: (1) although horizontal and vertical transports accounted for a considerable portion of process budgets, the net effects of transport processes exhibited negative contributions to the build-up of maximum O_3, and (2) the chemical process dominated the O_3 enhancement from morning to mid-afternoon, when O_3 concentrations usually reached the maximum level of the day.

3.3.2 Process analysis applied to regional O_3 pollution

In this section, the process analysis focuses on the whole PRD region with its daytime O_3 build-up in the ABL from 09:00 to 15:00 LST. On 16, 19, and 22 October (characterized by different near-ground flow conditions and O_3 pollution patterns; refer to Table 4), the chemical process played a dominant role in the O_3 enhancements over most of the area of the PRD, especially in the southern and western PRD where elevated O_3 was distributed around mid-afternoon. In contrast, the transport process (the sum of horizontal and vertical transports) exhibited less influence on the regional scale, except in isolated areas, where the large power plants or the busy harbors located and intensive NO_x emissions resulted in strong O_3 titration (Fig. 11). The dominant contribution of chemical production not only occurred on the days with different near-ground flow conditions, but also over the areas with different emission strengths (i.e. urban vs. rural).

The lower precursor emissions in Jiangmen and southwestern coastal areas (Fig. 2) indicate that the transport process might play an important role in maintaining the necessary levels of precursors involved in the elevated O_3 chemical production there. The regional distribution of NO_x contributed by the transport process, integrated over the depth of layers 1 to 7 and accumulated from late afternoon (17:00 LST) to the next morning (09:00 LST), is used to reflect the redistribution of NO_x from the source regions to the whole PRD (Fig. 12). The IPR results show that the transport process functions as a sink of NO_x in areas with intensive NO_x emissions (such as in urban areas of Guangzhou, Dongguan, Shenzhen, and Hong Kong), but as the dominant source of NO_x over the southern or southwestern PRD (especially in Jiangmen and the PRE), even if the accumulated time range is extended to 15:00 LST of the next afternoon.

The flow conditions influence the transport and redistribution of NO_x during the night and next morning (Fig. 12). From late afternoon to midnight on 15 and 21 October, southeasterly sea breezes developed and prevailed in the southern part of the PRD, and wind convergence appeared over Panyu, Jiangmen, and Zhongshan (Fan et al., 2008), which mixed the NO_x plumes from northern source areas (i.e. urban Guangzhou and Foshan) with plumes from southern areas (i.e. Dongguan, Shenzhen, and Hong Kong) inside the PRD; this hindered the transport of NO_x outside the PRD. After midnight, northerly or northeasterly wind again prevailed over the PRD, and the delayed NO_x plume was transported to the south and west, providing the majority of NO_x involved in O_3 enhancement by the daytime photochemical process in Jiangmen and southwestern coastal areas. The transport of NO_x from the late afternoon of 18 October to the morning of 19 October was mainly controlled by northerly winds and was not affected by the sea breeze, which resulted in less NO_x accumulation inside the PRD than what happened on the other two days.

The above process analysis not only exhibits the redistributions of precursors from night to the next morning, but also reveals the significance of O_3 chemical production on a large regional scale in the daytime under such close interactions among the precursor emissions, physical transport, and photochemical process.

3.4 Ozone production efficiency

As illustrated in Fig. 13, OPE shows significant spatial variations over the PRD. The calculated OPEs are 2–8 in most regions of the middle and western PRD, corresponding to the areas of high O_3 chemical production (Fig. 11a). Less efficiency (i.e. OPE values of 1–5) is shown in the urban areas of Guangzhou, Foshan, Shenzhen, and Hong Kong, characterized by intensive NO_x emissions, as well as downwind areas of the urban plumes under prevailing northeasterly flow. In contrast, high OPEs (larger than 11) are shown over upwind or rural areas with less NO_x source emissions (e.g. Huizhou, Zhaoqing, and Qingyuan).

For the period of 16–22 October, the average OPE values during 09:00–15:00 LST were 3.6 (2.9–4.0) at GDEMC, 4.9 (4.2–5.9) at Xinken, and 5.0 (3.3–7.3) at Donghu. NO_x exhibits lower catalysis efficiency at the urban GDEMC site because of intensive local NO_x emissions by vehicles and industrial activities. For the rural Xinken site, despite lower local emissions, the significant NO_x sources in neighboring areas (such as power plants along the southern coast of Dongguan and intense NO_x emissions in the western coastal area of Shenzhen and in Hong Kong) provide NO_x for local photochemical reactions, resulting in a similar level of OPE as that found at Donghu (urban site). The simulated OPEs at the super sites are comparable to those observed in urban Beijing, ranging from 3.9 to 9.7 (Chou et al., 2009), and those observed or modeled in US cities (Nummermacker et al., 1998; Kleinman et al., 2000) and in the Mexico City Metropolitan Area (Lei et al., 2007).

ACPD
9, 26833–26880, 2009

3.5 Sensitivity of O_3 to precursors

In this section, we first examine the response of surface O_3 to precursor emission reductions, averaged over 12:00–17:00 LST from 16 to 22 October (Fig. 14). Over the central inland PRD and the PRE and surrounding coastal areas (i.e. the region marked by the red ellipse in Fig. 14), O_3 levels decrease (by 0.006~0.019 ppm) with the reduction of only VOC emissions; however, O_3 levels increase (by 0.003~0.017 ppm) in most of the areas with the reduction of only NO_x emissions. Such O_3 changes suggest that O_3 formation was under a VOC-limited regime and was depressed by high NO_x levels in these urban areas and the immediate downwind areas during the campaign period, which is consistent with Zhang et al.'s (2008b) findings from an OBM at the GDEMC and Xinken sites. The O_3 levels are more sensitive to the perturbation of NO_x emissions but exhibit fewer changes with VOCs reductions in the rural southwestern PRD (i.e. the region marked by blue ellipse in Fig. 14), where less NO_x and low-to-moderate VOC emissions are distributed (see Fig. 2). The O_3 response supports the important role of NO_x regional transport to O_3 formation in the southwestern PRD, as obtained by the process analysis in Sect. 3.3.2. With reductions in both NO_x and VOCs emissions, O_3 levels decrease over most of the central and western PRD.

Next, we check the response of O_3 photochemical production rates to the perturbations of precursor emissions because of the critical influence of the chemical process on O_3 enhancement from low concentrations in morning to maximum levels in mid-afternoon over most parts of the central and western PRD. Figure 15a and b shows that the responses of the net chemical production rates of O_x [$P(O_x)$] are similar to the changes of O_3 in the central and western PRD (see Fig. 14a and b), except for the obvious decrease in the eastern PRD with the reduction of NO_x emissions (i.e. a clear NO_x-sensitive response). The distribution of the NO_x/NO_y ratio is also presented for understanding the responses of $P(O_x)$ (Fig. 15c). The VOC-sensitive area over the PRD generally corresponds to the areas of higher NO_x/NO_y ratios, whereas the decrease of $P(O_x)$ due to the reduction of NO_x emissions usually occurs in the regions

ACPD
9, 26833–26880, 2009

of lower NO_x/NO_y ratios, similar to results from the Mexico City Metropolitan Area (Lei et al., 2007). Generally, in and near urban cores, air plumes are exposed to fresh pollutants (high NO_x/NO_y ratios) and tend to fall into the VOC-limited regime and even the NO_x disbenefit regime (i.e. an increase in $P(O_x)$ resulting from a decrease in NO_x). However, in suburban and rural regions, air plumes tend to maintain low NO_x/NO_y due to the rapid removal of NO_x by the chemical process in the course of transport to those regions, and O_3 production also tends to shift from VOC-limited to NO_x-limited chemistry for the same reason (NARSTO, 2000).

We next further investigate the relationships between $P(O_x)$ changes and NO_x/NO_y ratios at the GDEMC, Xinken, Donghu, Kaiping, and Duanfen sites (Fig. 16). Although the distribution of NO_x/NO_y ratio shows significant difference (i.e. GDEMC is characterized by high ratios, but Kaiping and Duanfen are dominated by low values), the responses of $P(O_x)$ share some common features at the five sites. In the case of 25% reduction of VOCs emissions, the percentage change in $P(O_x)$ tends to increase from about −30% to 30% with the NO_x/NO_y ratio, whereas a decreasing tendency is obtained in the condition of NO_x emission reduction. The VOC benefit (i.e. a decrease in $P(O_x)$ resulting from a reduction in VOCs) and the NO_x disbenefit suggest an obvious VOC-limited chemistry under higher NO_x/NO_y conditions (>0.6, corresponding to fresh pollutants), whereas the opposite responses of $P(O_x)$ indicate the NO_x-limited regime occurring under lower NO_x/NO_y conditions (<0.3, corresponding to chemically aged pollutants). The range of the NO_x/NO_y ratio from about 0.4 to 0.6 seems to be a common transition between NO_x- and VOC-limited chemistry at all five sites.

4 Summary

The MM5/SMOKE/CMAQ modeling system was applied to investigate O_3 pollution over the PRD region during the PRIDE-PRD2004 campaign. Model performance was assessed by comparing simulated O_3, NO_2, and NMHC concentrations with measurements from two super sites (GDEMC and Xinken) of the campaign and from PRD

ACPD
9, 26833–26880, 2009

regional air quality monitoring networks. The model reasonably reproduces the ozone episodes observed during the 1-month campaign.

Elevated O_3 levels are usually observed in the southwestern inland PRD, PRE, and southern coastal areas, resulting from the intensive precursor emissions in the central PRD and the dominant northerly or easterly winds during October. Three evolution patterns of simulated surface O_3 are categorized based on the different near-ground flow conditions, and more than 75% of the days occurred under the interaction between weak synoptic forcing and local sea-land circulations.

For daytime O_3 evolution at the urban GDEMC site, the chemical process serves as sink in lower layers (0~80 m a.g.l.) but as a source in upper layers (80~1000 m a.g.l.). The significant chemical removal of O_3 near the surface is compensated by the contributions of vertical transport from upper layers and horizontal advection from upwind areas. The rural Xinken site is characterized by strong local circulations, resulting in significant vertical inflow and comparable horizontal outflow; in this area, photochemical production serves as a steady contributor during the daytime. The IPR results on overall O_3 evolution in the ABL over the PRD suggest that photochemical production is the dominant contributor to O_3 enhancement from 09:00 to 15:00 LST, and regions of high chemical production generally coincide with those of elevated O_3 levels.

The range of simulated OPE is 2–8 O_3 molecules per NO_x molecule oxidized in most areas of high O_3 chemical production. Through the transport process during nighttime and morning, O_3 precursors originating from different source regions are mixed and transported to downwind rural areas, where they are then involved in the daytime O_3 photochemical production. As demonstrated above, these close interactions among precursor emissions, physical transport, and photochemical production ultimately resulted in regional O_3 pollution over the southern and western PRD during the PRIDE-PRD2004 campaign.

The O_3 sensitivity to precursors was investigated by comparisons of simulated O_3 levels between the base case and emission-control scenarios. Formation of O_3 is VOC-limited and NO_x-depressed in the central inland PRD, PRE, and surrounding coastal

ACPD
9, 26833–26880, 2009

areas, whereas O_3 levels show more sensitivity to NO_x in the rural southwestern PRD. The significant spatial variations of O_3 production sensitivity show a close relationship to the chemical aging of air plumes. VOC-limited chemistry usually dominates in less chemically aged air ($NO_x/NO_y > 0.6$), whereas NO_x-limited chemistry generally occurs within chemically aged plumes ($NO_x/NO_y < 0.3$).

The spatial variation of O_3 formation sensitivity suggests a non-uniform precursor emission-reduction strategy for O_3 pollution control in sub-regions of the PRD. Considering the source emissions concentrated in urban areas and the significant precursor transport to downwind rural areas, reductions in both VOC and NO_x emissions, combined with more emphasis on VOC controls, appear to be practical for lowering the O_3 levels over the PRD region.

Acknowledgements. This work was supported by the National High Technology Research and Development Program of China (Grant No: 2006AA06A306), the National Basic Research Program of China (Grant No: 2002CB410801) and the European Commission Framework Programme 7 project CityZen (Grant No. 212095). The authors are grateful to Peter Louie (Hong Kong Environmental Protection Department) for supplying the emission data, to Shaojia Fan (Sun Yat-sen University) for supporting meteorological observation data, to Jia-Lin Wang (National Central University, Taiwan), Shaw Liu and Chih-Chung Chang (Academia Sinica, Taiwan) for providing NMHC online measurement data, and to Yang Zhang (North Carolina State University, Raleigh, USA) for her valuable suggestions.

References

Byun, D. and Schere, K. L.: Review of the governing equations, computational algorithms, and other components of the Models-3 Community Multiscale Air Quality (CMAQ) modeling system, Appl. Mech. Rev., 59, 51–77, 2006.

Cao, G., Zhang, X., Wang, D., and Zheng, F.: Inventory of atmospheric pollutants discharged from biomass burning in China continent, China Environmental Science, 25(4), 389–393, 2005.

Carter, W. P. L.: Documentation of the SAPRC-99 chemical mechanism for VOC reactivity

assessment, Final Report to California Air Resources Board, Contract No. 92-329 and 95-308, 2000.
Chan, C. Y. and Chan, L. Y.: Effect of meteorology and air pollutant transport on ozone episodes at a subtropical coastal Asian city, Hong Kong, J. Geophys. Res., 105(D16), 20707–20724, 2000.
Chan, C. K. and Yao, X.: Air pollution in mega cities in China, Atmos. Environ., 42, 1–42, 2008.
Chou, C. C. K., Liu, S. C., Lin, C. Y., Shiu, C. J., and Chang, K. H.: The trend of surface ozone in Taipei, Taiwan, and its causes: Implications for ozone control strategies, Atmos. Environ., 40, 3898–3908, 2006.
Chou, C. C. K., Tsai, C. Y., Shiu, C. J., Liu, S. C., and Zhu, T.: Measurement of NO_y during Campaign of Air Quality Research in Beijing 2006 (CAREBeijing-2006): Implications for the ozone production efficiency of NO_x, J. Geophys. Res., 114, D00G01, doi:10.1029/2008JD010446, 2009.
Ding, A., Wang, T., Zhao, M., Wang, T., and Li, Z. K.: Simulation of sea-breezes and a discussion of their implications on the transport air pollution during a multi-day ozone episode in the Pearl River Delta of China, Atmos. Environ., 12(29), 6737–6750, 2004.
Emery, C. A., Tai, E., and Yarwood, G.: Enhanced meteorological modeling and performance evaluation for two Texas ozone episodes, Project Report prepared for the Texas Natural Resource Conservation Commissions, ENVIRON International Corporation, Novato, CA, 2001.
Fan, S. J., Wang, B. M., Tesche, M., Engelmann, R., Althausen, A., Liu, J., Zhu, W., Fan, Q., Li, M. H., Ta, N., Song, L. L., and Leong, K. C.: Meteorological conditions and structures of atmospheric boundary layer in October 2004 over Pearl River Delta area, Atmos. Environ., 42, 6174–6186, 2008.
Gipson, L. G.: Science Algorithms of the EPA Models-3 Community Multiscale Air Quality (CMAQ) Modeling System: process analysis, EPA/600/R-99/030, US EPA, online available at: http://www.epa.gov/asmdnerl/CMAQ/ch16.pdf, 37 pp., 1999.
Gonçalves, M., Jiménez-Guerrero, P., and Baldasano, J. M.: Contribution of atmospheric processes affecting the dynamics of air pollution in South-Western Europe during a typical summertime photochemical episode, Atmos. Chem. Phys., 9, 849–864, 2009, http://www.atmos-chem-phys.net/9/849/2009/.
Grell, G. A., Dudhia, J., and Stanffer, D. R.: A description of the Fifth-generation Penn State/NCAR Mesoscale Model (MM5), NCAR Technical Note: NCAR/TN-398+STR, 1994.
Hanna, S. R. and Yang, R. X.: Evaluations of mesoscale models' simulations of near-surface

winds, temperature gradients, and mixing depths, J. Appl. Meteorol., 40(6), 1095–1104, 2001.
Houyoux, M. R., Vukovich, J. M., Coats Jr., C. J., Wheeler, N. J. M., and Kasibhatla, P.: Emission inventory development and processing for the seasonal model for regional air quality, J. Geophys. Res., 105(D7), 9079–9090, 2000.
Huang, J. P., Fung, J. C. H., Lau, A. K. H., and Qin, Y.: Numerical simulation and process analysis of typhoon-related episodes in Hong Kong, J. Geophys. Res., 110, D05301, doi:10.1029/2004JD004914, 2005.
Huang, J. P., Fung, J. C. H., and Lau, A. K. H.: Integrated processes analysis and systematic meteorological classification of ozone episodes in Hong Kong, J. Geophys. Res., 111, D20309, doi:10.1029/2005JD007012, 2006.
Jang, J. C., Jeffries, H. E., Byun, D., and Pleim, J. E.: Sensitivity of ozone to model grid resolution – I. Application of high-resolution regional acid deposition model, Atmos. Environ., 21, 3085–3100, 1995.
Jeffries, H. E. and Tonnesen, S.: A comparison of two photochemical reaction mechanisms using mass balance and process analysis, Atmos. Environ., 28, 2991–3003, 1994.
Kleinman, L. I., Daum, P. H., Imre, D. G., Lee, J. H., Lee, Y. N., Nunnermacker, L. J., Springston, S. R., Weinstein-Lloyd, J., and Newman, L.: Ozone production in the New York City urban plume, J. Geophys. Res., 105(D11), 14495–14511, 2000.
Lam, K. S., Wang, T. J., Wu, C. L., and Li, Y. S.: Study on an ozone episode in hot season in Hong Kong and transboundary air pollution over Pearl River Delta region of China, Atmos. Environ., 39, 1967–1977, 2005.
Lei, W., de Foy, B., Zavala, M., Volkamer, R., and Molina, L. T.: Characterizing ozone production in the Mexico City Metropolitan Area: a case study using a chemical transport model, Atmos. Chem. Phys., 7, 1347–1366, 2007, http://www.atmos-chem-phys.net/7/1347/2007/.
Liu, H. and Chan, J. C. L.: An investigation of air-pollutant patterns under sea-land breezes during a severe air-pollution episode in Hong Kong, Atmos. Environ., 36, 591–601, 2002.
Liu, J. F., Zhao, J., Li, T. T., Bai, Y. H., and Liu, Z. R.: Establishment of Chinese anthropogenic source volatile organic compounds emission inventory, China Environmental Science, 28(6), 496–500, 2008a.
Liu, Y., Shao, M., Lu, S., Chang, C.-C., Wang, J.-L., and Chen, G.: Volatile Organic Compound (VOC) measurements in the Pearl River Delta (PRD) region, China, Atmos. Chem. Phys., 8,

1531–1545, 2008b, http://www.atmos-chem-phys.net/8/1531/2008/.
Lo, J. C. F., Lau, A. K. H., Fung, J. C. H., and Chen, F.: Investigation of enhanced cross-city transport and trapping of air pollutants by coastal and urban land-sea breeze circulations, J. Geophys. Res., 111, D14104, doi:10.1029/2005JD006837, 2006.
NARSTO: An Assessment of Tropospheric Ozone Pollution: A North American Perspective, The NARSTO Synthesis Team, Palo Alto, CA, 2000.
Nunnermacker, L. J., Imre, D., Daum, P. H., Kleinman, L., Lee, Y. N., Lee, J. H., Springston, S. R., Newman, L., Weinstein-Lloyd, J., Luke, W. T., Banta, R., Alvarez, R., Senff, C., Sillman, S., Holdren, M., Keigley, G. W., and Zhou, X.: Characterization of the Nashville urban plume on July 3 and July 18, 1995, J. Geophys. Res., 103(D21), 28129–28148, 1998.
Seinfeld, J. H. and Pandis, S. N.: Atmospheric chemistry and physics: From air pollution to climate change (Second edition), John Wiley & Sons, Inc., Hoboken, New Jersey, 2006.
Shao, M., Zhang, Y. H., Zeng, L. M., Tang, X. Y., Zhang, J., Zhong, L. J., and Wang, B. G.: Ground-level ozone in the Pearl River Delta and the roles of VOC and NO_x in its production, J. Environ. Manage., 90, 512–518, 2009.
Sillman, S.: The use of NO_y, H_2O_2, and HNO_3 as indicators for ozone-NO_x-hydrocarbon sensitivity in urban locations, J. Geophys. Res., 100(D7), 14175–14188, 1995.
Sillman, S. and He, D. Y.: Some theoretical results concerning O3-NO_x-VOC chemistry and NO_x-VOC indicators, J. Geophys. Res., 107(D22), 4659, doi:10.1029/2001JD001123, 2002.
Streets, D. G., Bond, T. C., Carmichael, G. R., Fernandes, S. D., Fu, Q., He, D., Klimont, Z., Nelson, S. M., Tsai, N. Y., Wang, M. Q., Woo, J. H., and Yarber, K. F.: An inventory of gaseous and primary aerosol emissions in Asia in the year 2000, J. Geophys. Res., 108(D21), 8809, doi:10.1029/2002JD003093, 2003.
Song, X. Y. and Xie, S. D.: Development of vehicular emission inventory in China, Environ. Sci., 27(6), 1041–1045, 2006.
Wang, J. L., Wang, C. H., Lai, C. H., Chang, C. C., Liu, Y., Zhang, Y. H., Liu, S., and Shao, M.: Characterization of ozone precursors in the Pearl River Delta by time series observation of non-methane hydrocarbons, Atmos. Environ., 42, 6233–6246, 2008a.
Wang, K., Zhang, Y., Jang, C., Phillips, S., and Wang, B. Y.: Modeling intercontinental air pollution transport over the trans-Pacific region in 2001 using the Community Multiscale Air Quality modeling system, J. Geophys. Res., 114, D04307, doi:10.1029/2008JD010807, 2009.
Wang, T., Poon, C. N., Kwok, Y. H., and Li, Y. S.: Characterizing the temporal variability and

emission patterns of pollution plumes in the Pearl River Delta of China, Atmos. Environ., 37, 3539–3550, 2003.
Wang, T., Wu, Y. Y., Cheung, T. F., and Lam, K. S.: A study of surface ozone and the relation to complex wind flow in Hong Kong, Atmos. Environ., 35, 3203–3215, 2001.
Wang, T. J., Lam, K. S., Xie, M., Wang, X. M., Carmichael, G., and Li, Y. S.: Integrated studies of a photochemical smog episode in Hong Kong and regional transport in the Pearl River Delta of China, Tellus, 58B, 31–40, 2006.
Wang, W., Ren, L. H., Zhang, Y. H., Chen, J. H., Liu, H. J., Bao, L. F., Fan, S. J., and Tang, D. G.: Aircraft measurements of gaseous pollutants and particulate matter over Pearl River Delta in China, Atmos. Environ., 42, 6187–6202, 2008b.
Wang, X., Carmichael, G., Chen, D., Tang, Y., and Wang, T.: Impacts of different emission sources on air quality during March 2001 in the Pearl River Delta (PRD) region, Atmos. Environ., 39, 5227–5241, 2005.
Wei, X. L., Li, Y. S., Lam, K. S., Wang, A. Y., and Wang, T. J.: Impact of biogenic VOC emissions on a tropical cyclone-related ozone episode in the Pearl River Delta region, China, Atmos. Environ., 41, 7851–7864, 2007.
Xu, J., Zhang, Y. H., Fu, J. S., Zheng, S. Q., and Wang, W.: Process analysis of typical summertime ozone episodes over the Beijing area, Sci. Total Environ., 399, 147–157, 2008.
Yu, S., Mathur, R., Kang, D., Schere, K., and Tong, D.: A study of the ozone formation by ensemble back trajectory-process analysis using the Eta-CMAQ forecast model over the northeastern US during the 2004 ICARTT period, Atmos. Environ., 43, 355–363, 2009.
Zhang, J., Wang, T., Chameides, W. L., Cardelino, C., Kwok, J., Blake, D. R., Ding, A., and So, K. L.: Ozone production and hydrocarbon reactivity in Hong Kong, Southern China, Atmos. Chem. Phys., 7, 557–573, 2007, http://www.atmos-chem-phys.net/7/557/2007/.
Zhang, Y., Liu, P., Queen, A., Misenis, C., Pun, B., Seigneur, C., and Wu, S.-Y.: A comprehensive performance evaluation of MM5-CMAQ for the Summer 1999 Southern Oxidants Study episode – Part II: Gas and aerosol predictions, Atmos. Environ., 40, 4839–4855, 2006.
Zhang, Y., Vijayaraghavan, K., Wen, X.-Y., Snell, H. E., and Jacobson, M. Z.: Probing into regional O_3 and PM pollution in the US, Part I, A 1-year CMAQ simulation and evaluation using surface and satellite data, J. Geophys. Res., 114, D22304, doi:10.1029/2009JD011898, 2009a.
Zhang, Y., Wen, X.-Y., Wang, K., Vijayaraghavan, K., and Jacobson, M. Z.: Probing into

regional O_3 and PM pollution in the US, Part II, An examination of formation mechanisms through a process analysis technique and sensitivity study, J. Geophys. Res., 114, D22305, doi:10.1029/2009JD011900, 2009b.

Zhang, Y. H., Hu, M., Zhong, L. J., Wiedensohler, A., Liu, S. C., Andreae, M. O., Wang, W., and Fan, S. J.: Regional integrated experiments on air quality over Pearl River Delta 2004 (PRDIE-PRD2004): Overview, Atmos. Environ., 42, 6157–6173, 2008a.

Zhang, Y. H., Su, H., Zhong, L. J., Cheng, Y. F., Zeng, L. M., Wang, X. S., Xiang, Y. R., Wang, J. L., Gao, D. F., Shao, M., Fan, S. J., and Liu, S. C.: Regional ozone pollution and observation-based approach for analyzing ozone-precursor relationship during the PRIDE-PRD2004 campaign, Atmos. Environ., 42, 6203–6218, 2008b.

Table 1. Summary of annual anthropogenic emissions of NO_x and VOCs by source category over the PRD in 2004 (kilotons/yr).

Source category	NO_x	VOCs
Power generation point source	294	34
Mobile source	348	545
Industrial source	52	20
Domestic and commercial fuel combustion source	36	73
Solvent and petroleum evaporation source	0	345
Agriculture source and others	11	105
Total	742	1122

ACPD
9, 26833–26880, 2009

Table 2. Quantitative performance statistics for the MM5-simulated meteorological parameters in the 4-km domain against surface observations during 1–31 October 2004.

Meteorological variable	Statistical parameter	Performance
Surface wind speed	RMSE* (m/s)	1.64
	Bias (m/s)	0.27
	IOA**	0.66
Surface wind direction	Gross Error (deg.)	38.11
	Bias (deg.)	0.56
Surface temperature	Gross Error (K)	1.98
	Bias (K)	0.39
	IOA	0.85
Surface humidity	Gross Error (g/kg)	1.62
	Bias (g/kg)	−1.24
	IOA	0.64

* RMSE stands for the root mean square error.
** IOA stands for the index of agreement (Emery et al., 2001).

Table 3. CMAQ performance statistics for the simulated hourly concentrations of surface O_3 against observations* over the PRD during 4–31 October 2004.

Number of data pairs	Correlation coefficient	NMB (%)	NME (%)
3771	0.60	−17.4	26.4

* with a cut-off of observations below 40 ppb.

ACPD
9, 26833–26880, 2009

Table 4. Classification of O_3 pollution days into three evolution patterns in the PRD during 4–31 October 2004.

Pattern	Date
1st category	4, 5, 8, 18, 19, 25, 26
2nd category	6, 7, 9, 10, 11, 12, 14, 15, 16, 17, 20, 24, 27
3rd category	13, 21, 22, 23, 28, 29, 30, 31

Table 5. Summary of the average accumulated contributions of each process to O_3 formation over the depth of layers 1 to 7 for the period of 09:00 to 15:00 LST during 16–22 October 2004 at the GDEMC, Xinken, and Donghu sites (ppm/6 h).

Site	CHEM*	HTRA	VTRA	DDEP	NETC
GDEMC	0.072	0.004	−0.030	−0.002	0.044
Xinken	0.055	−0.031	0.025	0.000	0.049
Donghu	0.082	−0.021	0.016	−0.002	0.075

* CHEM: chemical process; HTRA: horizontal transport, the net effect of horizontal advection and diffusion; VTRA: vertical transport, the net effect of vertical advection and diffusion; DDEP: dry deposition; NETC: net change due to all processes.

ACPD
9, 26833–26880, 2009

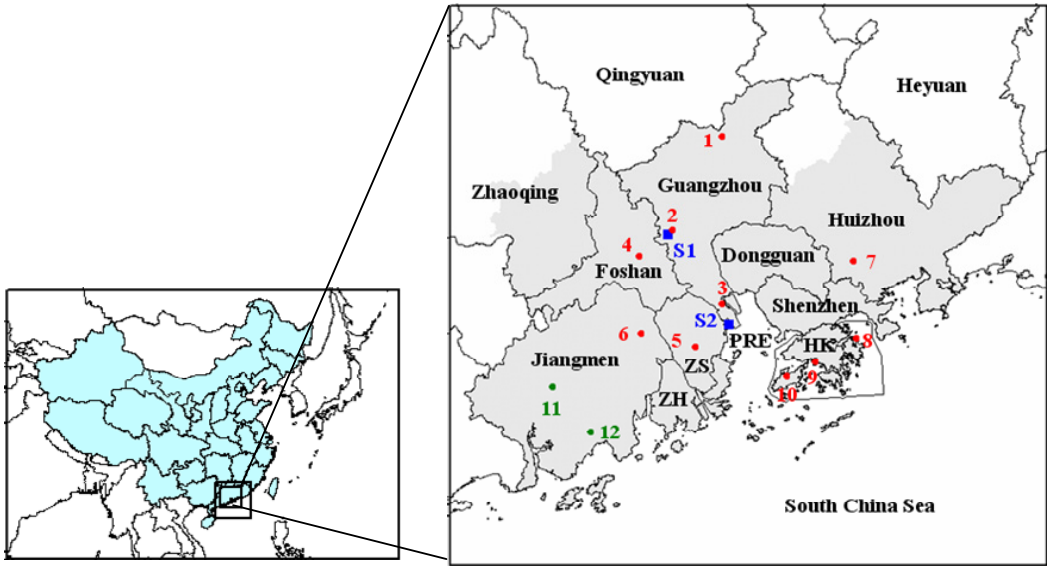

Fig. 1. (a) The 36-, 12-, and 4-km domains for CMAQ simulation; **(b)** distributions of monitoring sites in the 4-km domain. Two super sites are labeled in blue: S1-GDEMC, S2-Xinken; the PRD air quality monitoring networks are labeled in red numbers: 1-Tianhu, 2-Luhu, 3-Wanqingsha, 4-Huijingcheng, 5-Zimaling, 6-Donghu, 7-Jinguowan, 8-Tap Mun, 9-Tsuen Wan, and 10-Tung Chung; the sites labeled in green numbers (11-Kaiping and 12-Duanfen) are used to investigate the air quality in the southwestern inland and coastal areas of the PRD, although no observation data were collected at these sites during the PRIDE-PRD2004 campaign. The PRD region is the gray area on the map; the names of some sub-regions are abbreviated: ZS-Zhongshan, ZH-Zhuhai, HK-Hong Kong, PRE-Pearl River estuary).

ACPD
9, 26833–26880, 2009

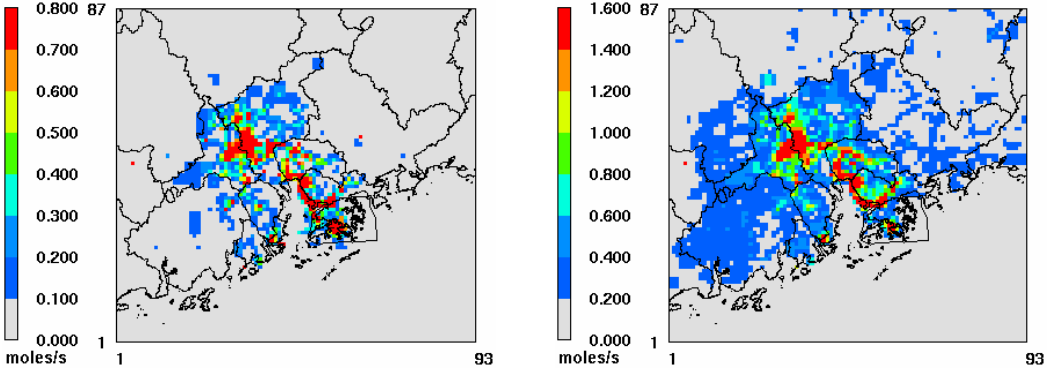

(a) (b)

Fig. 2. NO_x **(a)** and VOC **(b)** emissions in the 4-km grid at 12:00 LST on 16 October 2004.

ACPD
9, 26833–26880, 2009

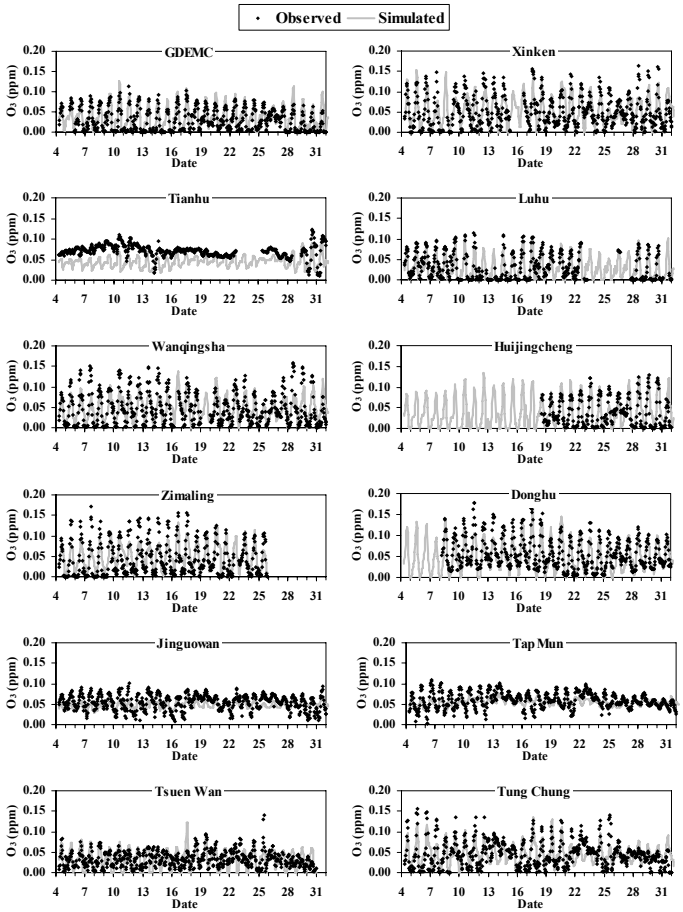

Fig. 3. Time series of simulated surface O_3 against that observed at PRD monitoring sites during 4–31 October 2004.

ACPD
9, 26833–26880, 2009

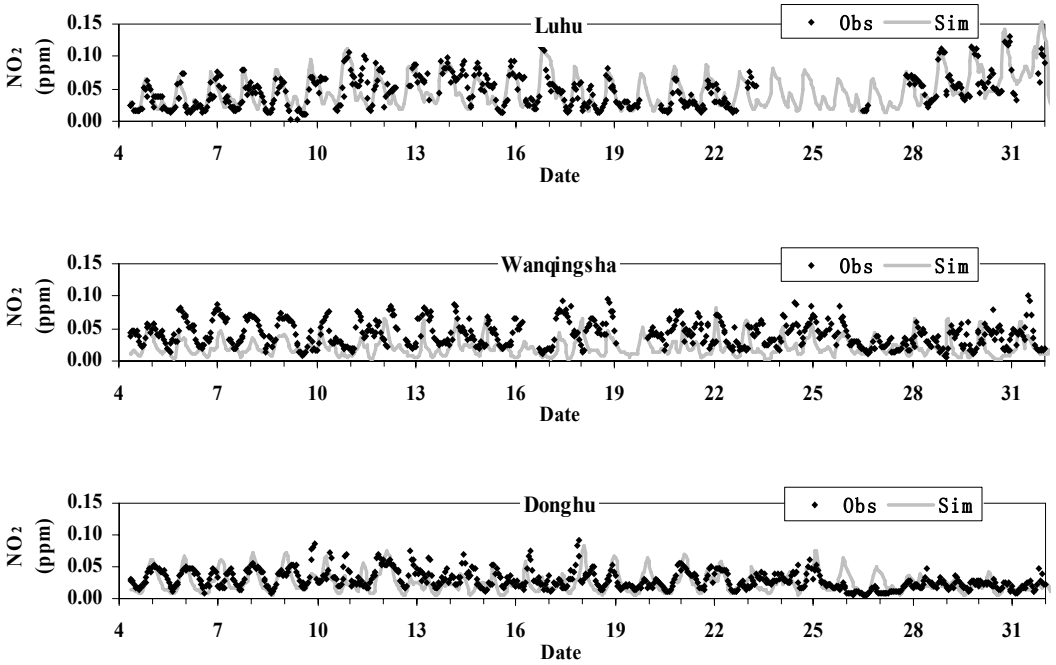

Fig. 4. Comparison of observed and simulated NO_2 at the Luhu, Wanqingsha, and Donghu sites.

ACPD
9, 26833–26880, 2009

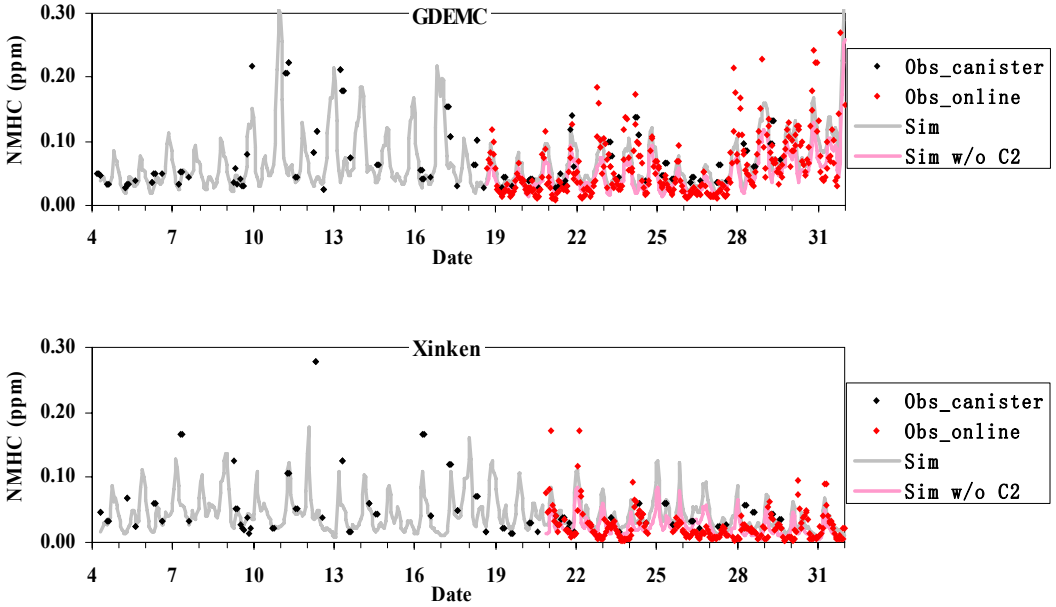

Fig. 5. Comparison of observed and simulated NMHC at the GDEMC and Xinken sites.

ACPD
9, 26833–26880, 2009

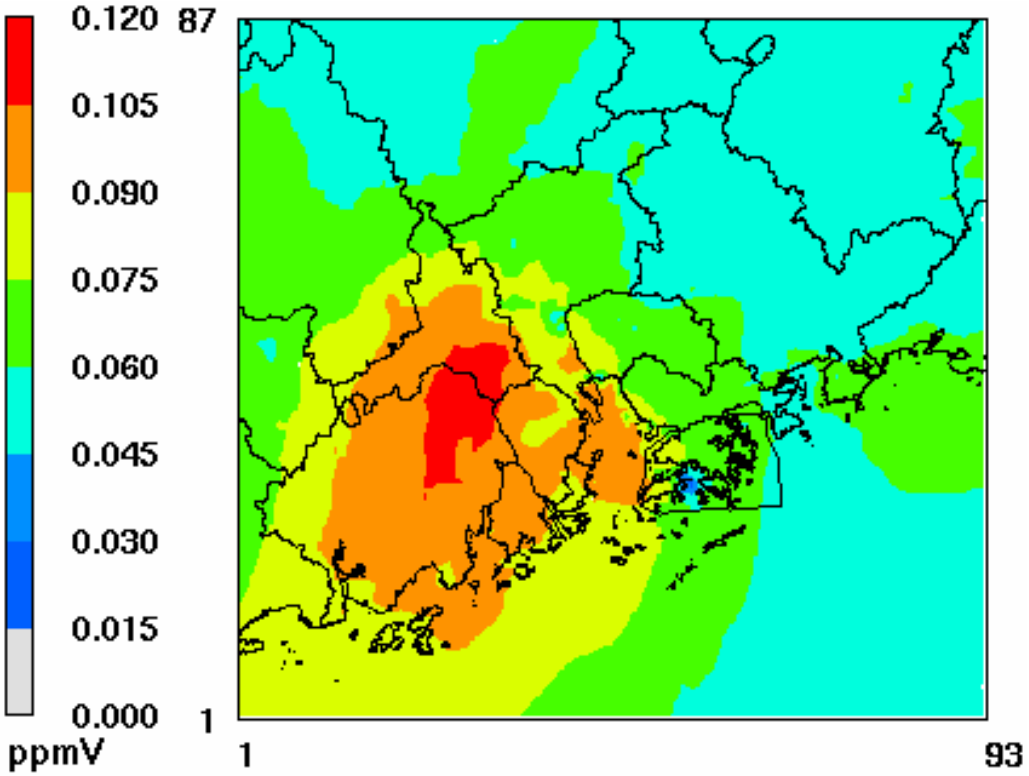

Fig. 6. Average hourly simulated surface O_3 at 15:00 LST during October 2004.

ACPD
9, 26833–26880, 2009

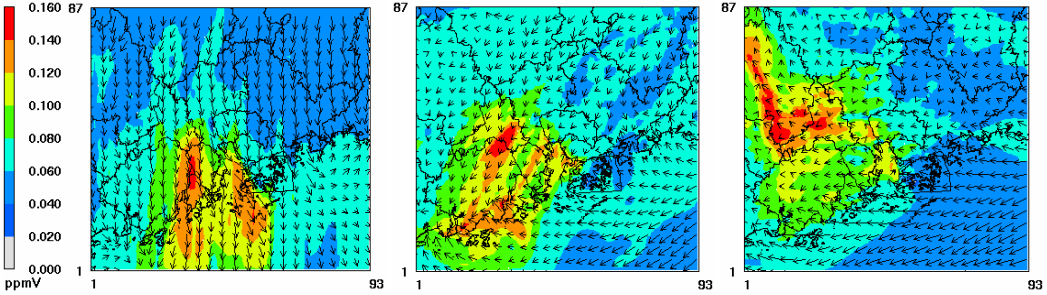

Fig. 7. Simulated surface O_3 concentrations superimposed with the wind fields at 15:00 LST on **(a)** 19 October, **(b)** 16 October, and **(c)** 29 October, taken as examples of the three O_3 evolution patterns, respectively.

ACPD
9, 26833–26880, 2009

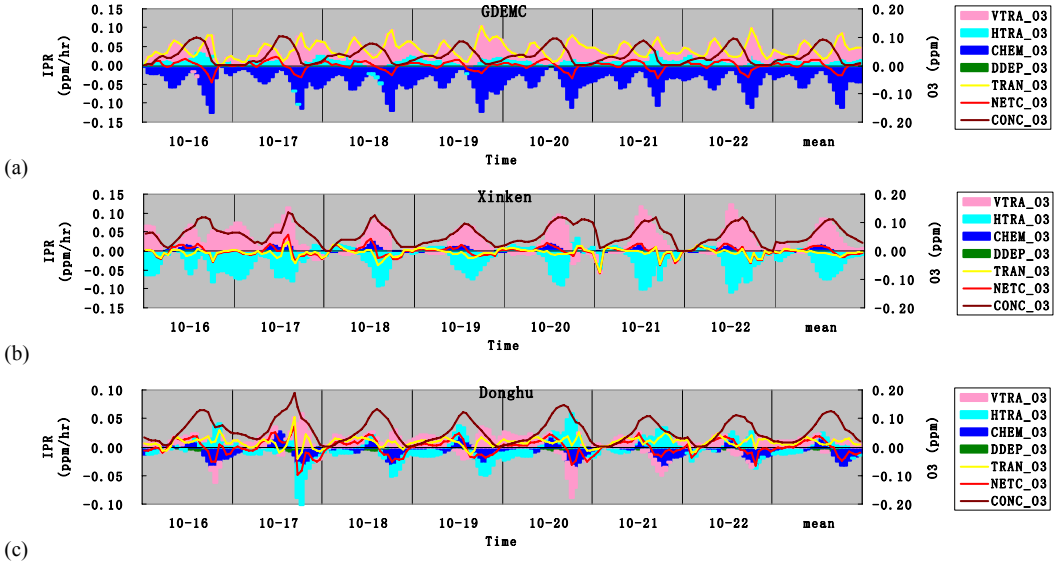

Fig. 8. Daily variations of O_3 concentration and hourly O_3 change rates due to various atmospheric processes in the lowest three layers (0–80 m a.g.l.) at **(a)** GDEMC, **(b)** Xinken, and **(c)** Donghu from 16–22 October 2004. (VTRA: vertical transport, the net effect of vertical advection and diffusion; HTRA: horizontal transport, the net effect of horizontal advection and diffusion; TRAN: transport, the net effect of VTRA and HTRA; DDEP: dry deposition; CHEM: chemical process; NETC: the net change of hourly O_3 due to all atmospheric processes; CONC: instantaneous O_3 concentration at the end of each hour).

ACPD
9, 26833–26880, 2009

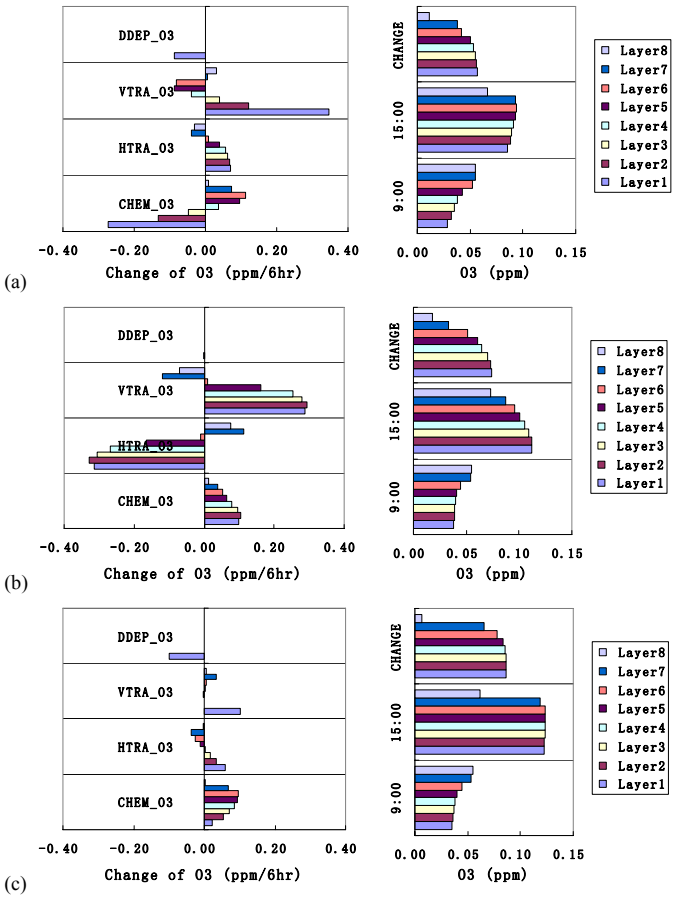

Fig. 9. O_3 change rates due to various atmospheric processes for layers 1 to 8 (left) and evolution of O_3 vertical profiles (right) at **(a)** GDEMC, **(b)** Xinken, and **(c)** Donghu from 09:00 to 15:00 LST averaged for 16–22 October 2004. (VTRA: vertical transport, the net effect of vertical advection and diffusion; HTRA: horizontal transport, the net effect of horizontal advection and diffusion; DDEP: dry deposition; CHEM: chemical process; CHANGE: the change of O_3 concentrations from 09:00 to 15:00 LST).

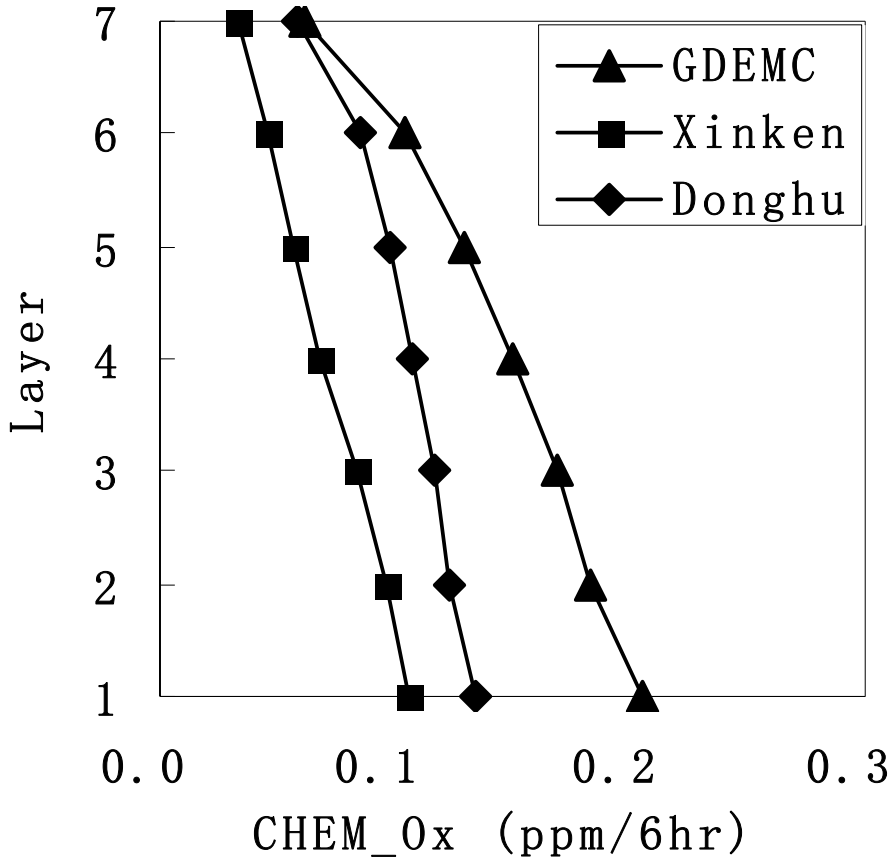

Fig. 10. Changes in O_x due to the chemical process at GDEMC, Xinken, and Donghu in the ABL (for layers 1 to 7) from 09:00 to 15:00 LST averaged for 16–22 October 2004. (O_x is estimated by O_3+NO_2).

ACPD
9, 26833–26880, 2009

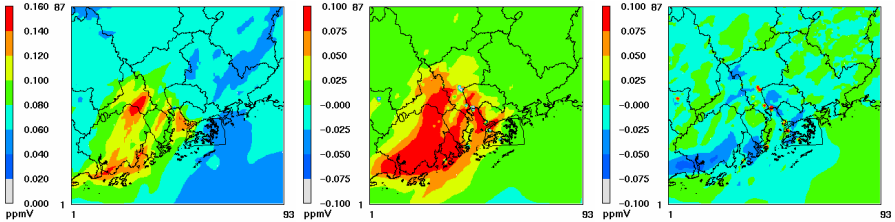

(a)

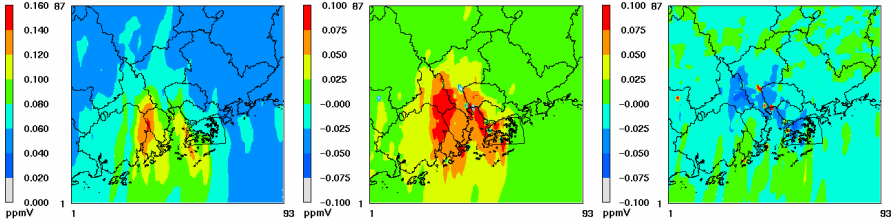

(b)

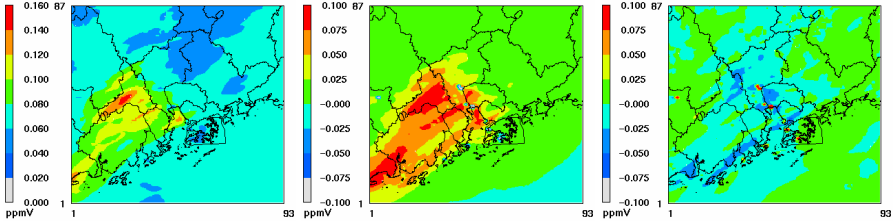

(c)

Fig. 11. Regional distributions of O_3 concentrations at 15:00 LST (left) and the accumulated contributions of the chemical process (center) and physical transport (right) from 09:00 to 15:00 LST over the depth of layers 1 to 7 on **(a)** 16 October, **(b)** 19 October, and **(c)** 22 October 2004.

ACPD
9, 26833–26880, 2009

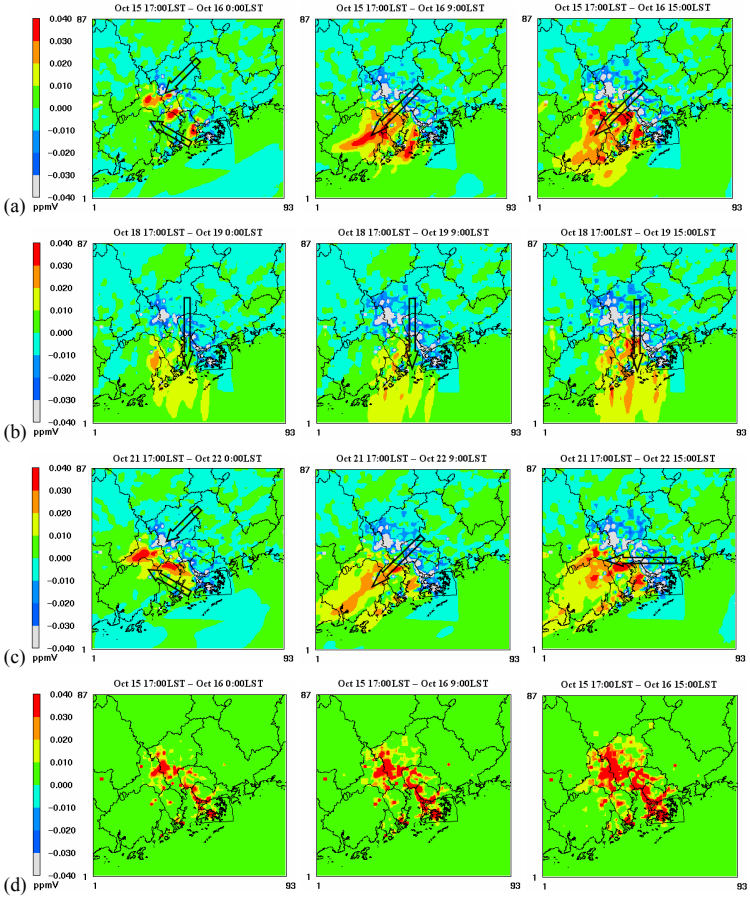

Fig. 12. **(a)**, **(b)** and **(c)** The accumulated contributions to NO_x by the transport process over the depth of layers 1 to 7 from 17:00 to 00:00 (left), 09:00 (center), and 15:00 LST (right) of the next day. The arrows show the near-ground dominant wind directions during the periods of 17:00–24:00 LST (left), 00:00–9:00 LST (center), and 09:00–15:00 LST (right). **(d)** The accumulated NO_x emissions in the same time range and vertical layers during 15–16 October are shown for comparison.

ACPD
9, 26833–26880, 2009

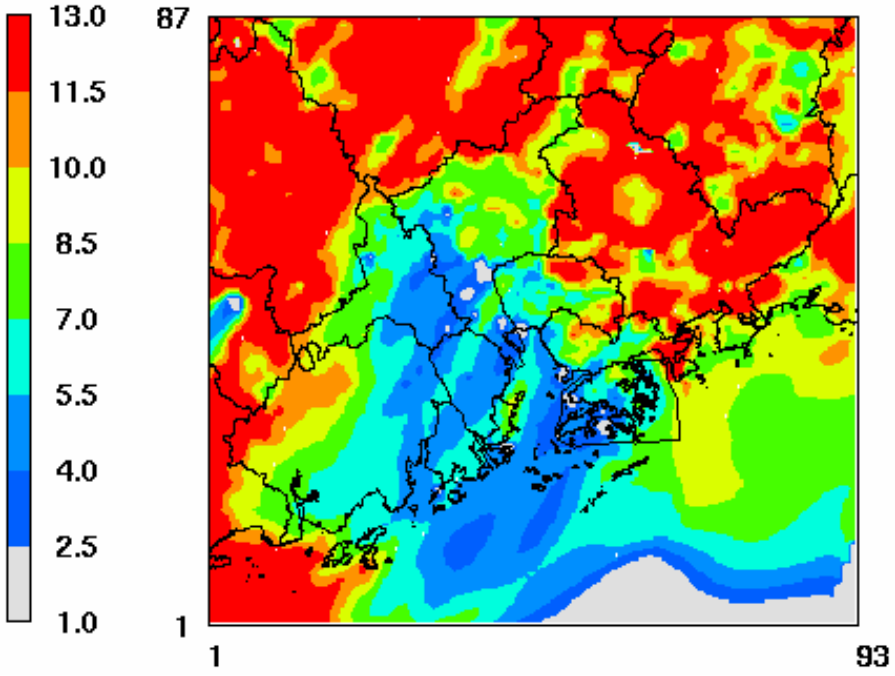

Fig. 13. Regional distribution of OPE calculated based on the overall chemical production of O_3 and NO_z over the lowest seven layers from 09:00 to 15:00 LST on 16 October 2004.

ACPD
9, 26833–26880, 2009

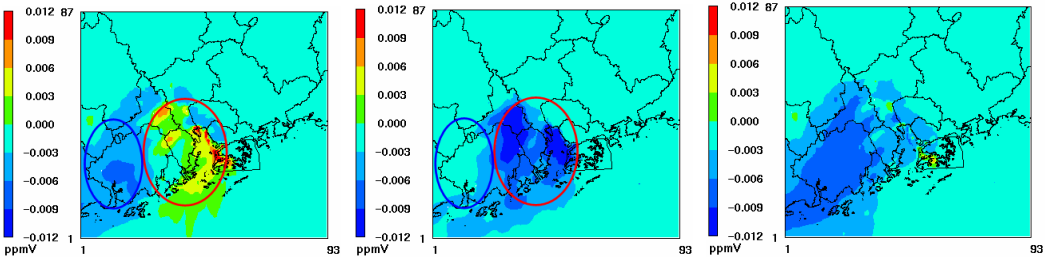

Fig. 14. Surface O_3 change averaged over 12:00–17:00 LST on 16–22 October 2004 due to a 25% reduction in anthropogenic emissions of **(a)** NO_x only, **(b)** VOCs only, and **(c)** both NO_x and VOCs.

ACPD
9, 26833–26880, 2009

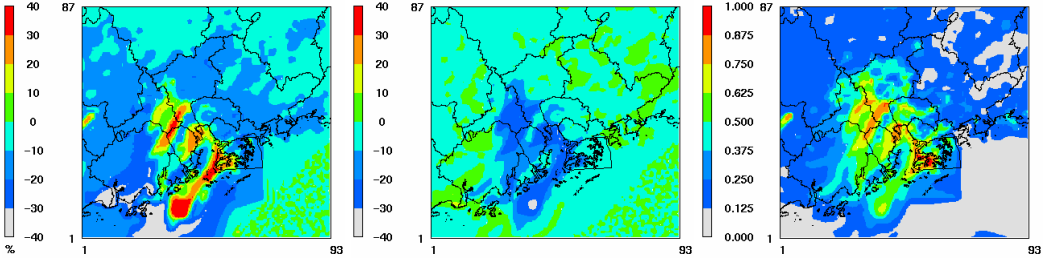

Fig. 15. Regional distribution of the percentage change in $P(O_x)$ due to a 25% reduction in anthropogenic emissions of NO_x only **(a)**, VOCs only **(b)**, and the NO_x/NO_y ratio in the base case run **(c)** in the surface layer during 12:00–13:00 LST on 16 October 2004.

ACPD
9, 26833–26880, 2009

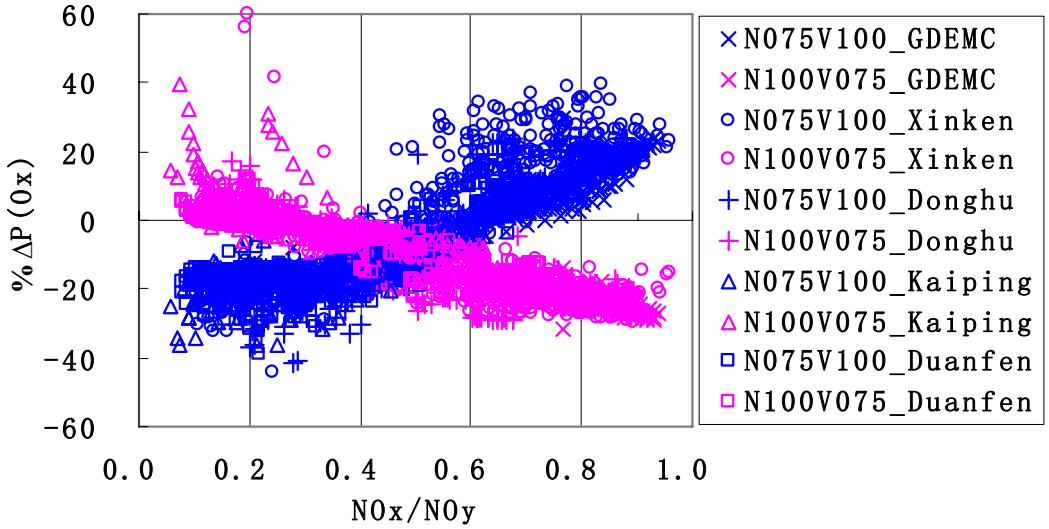

Fig. 16. The percentage change in $P(O_x)$ due to a 25% reduction in anthropogenic emissions of NO_x (N075V100) and VOCs (N100V075) as a function of the NO_x/NO_y ratio at the GDEMC, Xinken, Donghu, Kaiping, and Duanfen sites from layers 1 to 7 for the period of 09:00–17:00 LST during 16–22 October 2004.

ACPD
9, 26833–26880, 2009